Journal of Energy Storage 21 (2019) 156–162

Contents lists available at ScienceDirect

Journal of Energy Storage

journal homepage: www.elsevier.com/locate/est

Facile, cost-effective and eco-friendly green synthesis method of MnO_2 as storage electrode materials for supercapacitors

Hanaa M. Abuzeid[a], Safaa A. Elsherif[b], Nabil A. Abdel Ghany[b], Ahmed M. Hashem[a,*]

[a] National Research Centre, Inorganic Chemistry Department, 33 El Bohouth St., (former El Tahrir St.), Dokki-Giza 12622, Egypt
[b] National Research Centre, Physical Chemistry Department, 33 El Bohouth St., (former El Tahrir St.), Dokki-Giza 12622, Egypt

ARTICLE INFO

Keywords:
MnO_2
Nanaosized
Capacitors
Green synthesis
Energy

ABSTRACT

Orange by-products e.g. orange peel and the extract of orange juice are used as sources for biological antioxidants such as ascorbic acid, flavonoids, phenolic compounds and pectins. In this study these antioxidants were successfully used to prepare nanosized materials of α-MnO_2 by cost effective and eco-friendly green chemistry method. The prepared oxides of MnO_2 which have unique properties as a storage cathode material were tested as a pseudocapacitor electrode materials in this study. X-ray powder diffraction (XRD) confirmed the structure of α-MnO_2 for the prepared samples. Thermal behavior of prepared oxides was tested using thermogravimetric analysis (TGA). Transmission electron microscopy (TEM) showed the nanosized nature of the prepared oxides. N_2- adsorption–desorption isotherms and pore-size distributions of prepared oxides showed that the surface areas are 5.63 and 8.40 $m^2. g^{-1}$ for sample prepared from the extract of orange juice (OJ-MnO_2) and that prepared from the extract of orange peel (OP-MnO_2), respectively. Better electrochemical properties are obtained for OP-MnO_2, the capacitance of OP-MnO_2 (139 F/g) is more than two times and half that obtained for OJ-MnO_2 (50 F/g) at the current density 0.5 A/g.

1. Introduction

Fossil fuels as non-renewable source of energy became unable to meet the human need for energy especially with the rapid progress of the human science and technology. Environmental problems arising from using this pollutant source of energy push the research community to find an alternative renewable and clean source of energy [1–6]. These alternative sources can be obtained from energy storage devices that have high power, energy densities. Batteries, fuel cells and supercapacitors which have wide applications, friendliness and sustainable nature are the subject of big interest [7,8]. To meet the demand of using more energy current research focuses on the high energy density batteries and the high power density supercapacitors (SCs) [9]. State of the art lithium ion batteries which can store high amount of energy are suffered from low power density and rather short cycle life [10,11].

Supercapacitors or electrochemical capacitors as energy storage devices can give high power and can also deliver energy in short period of time unlike batteries. These devices are required for high-power delivery applications e.g. electric/hybrid electric vehicles, backup memories, digital products, airplane emergency doors, micro-devices, mobile devices, and next- generation portable electronics. This because they are cheap, need little maintenance, safe, require short charging time and have long cycle life [12]. Comparing to lithium ion batteries supercapacitors have lower energy density but they can reduce the gap between high energy density of the batteries and high power density of dielectric capacitor [13–15].

There are two types of supercapacitors classified according to the mechanism of charge storage: The first one is electrochemical double layer capacitor (EDLCs) and the other is pseudocapacitor (PDCs) [16,17]. In EDLCs energy is stored through electrostatic charge accumulated at the electrode-electrolyte interface [18]. In PDCs the energy is stored from combination the electrostatic charge accumulated at the electrode-electrolyte interface the fast faradaic redox reaction at or near the electrode materials [17].

Electrode materials have a direct impact on the behavior of supercapacitors [19]. In (EDLCs) carbon-based materials are used to store capacity via electrical charge at electrode / electrolyte interface. But in PDCs transition metal oxides e.g MnO_2 [20], Co_3O_4 [21], RuO_2, [22] V_2O_5, etc [23,24] are used as storage electrodes and yield specific capacitance through reversible Faradic redox reaction process occurred on electrode surface.

Manganese dioxide (MnO_2) as one of these transition metal oxides is used as a storage cathode material in battery technologies. This oxide has attracted an attention also as a pseudocapacitor electrode material

* Corresponding author.
E-mail address: ahmedh242@yahoo.com (A.M. Hashem).

https://doi.org/10.1016/j.est.2018.11.021
Received 29 August 2018; Received in revised form 25 October 2018; Accepted 22 November 2018
Available online 28 November 2018
2352-152X/

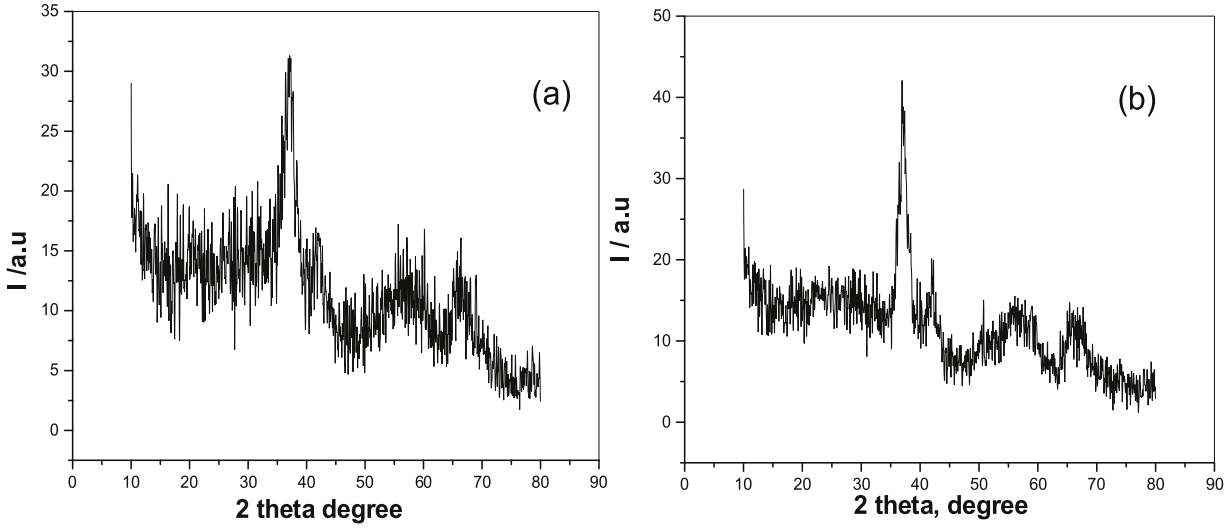

Fig. 1. X-ray powder diffraction patterns of synthesized MnO_2 (a) OP-MnO_2 with extract of orange's peel and (b) OJ-MnO_2 with extract of orange's juice".

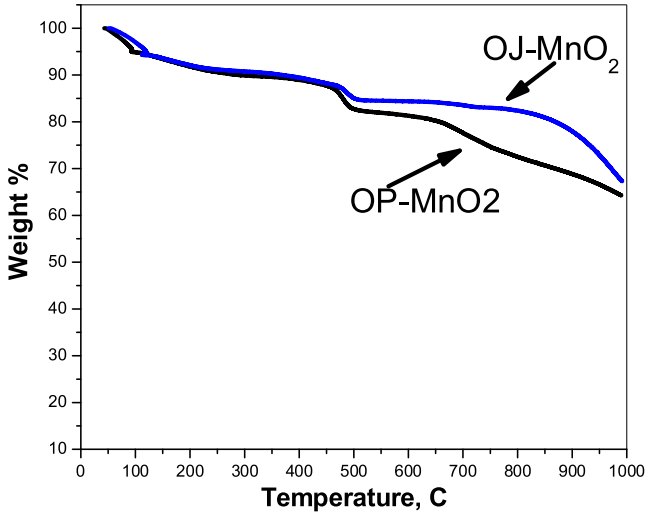

Fig. 2. Thermal gravimetric analysis of green synthesized samples OJ-MnO_2 and OP-MnO_2.

because it has high specific Faradic capacitance [6,8,19,20]. This oxide is abundant and cheap and has high reversibility, rapid diffusion behavior and desirable electrochemical properties…etc [25,26]. The charge storage mechanism of MnO_2 electrode is attributed to Faradic reaction due to the shuttle redox reactions between Mn^{4+} and Mn^{3+} in outer active surface sites, which are promoted through the insertion of electrolyte cations and protons [27,28]. Supercapacitors used MnO_2 as positive electrode and carbon material as negative electrode, gave higher energy density than supercapacitors based only on carbon materials [29].

There are different crystallographic forms of MnO_2 e.g. α, β, γ, ζ, λ and δ forms.

The crystal structure of MnO_2 can be classified by its tunnel size. α-MnO_2 is a stable form and has a wide 2 × 2 tunnels (~4.6 Å) which facilitates facile diffusion of large-size electrolyte cations (Na^+ or K^+) and hence achieving a high specific capacitance [30].

Some studies tried to prepare high surface area MnO_2 to enhance its specific capacitance [31,32]. These studies used sol-gel pyrolysis [33], hydrothermal methods [34], hydrothermal pyrolysis methods [35], refluxing methods [36] to obtain nanosized MnO_2. Some unavoidable disadvantages of these complicated methods such as high temperature, time consumption and high pressure cannot be alleviated [37]. Recently MnO_2 was obtained by green method which reduce the consumption of energy, the entire cost, the toxicity of solvents and organic substrates and used also the disposable by-products [38].

Oranges as citrus fruit constitute about 60% of the total world production and Egypt produces million tons of these citrus fruits. Huge quantities of residues e.g. orange peel as a primary byproduct is resulted from the industrial extraction of citrus juice. These big by-products amount of orange peel should be further processed to avoid many hazardous impacts and serious environmental pollution [39–41]. Juices and peels of these citrus fruits are important sources of biological antioxidants such as ascorbic acid, flavonoids, phenolic compounds and pectins [42].

The main constituents of the orange juice are organic acids, sugars, and phenolic compounds. Citric, malic, and ascorbic acids are the main organic acids found in orange juice whereas sucrose, glucose, and fructose are the main sugars found in this juice. The third constituent of the orange juice is phenolic compounds e.g.hydroxycinnamic acids, flavanones, hydroxybenzoic acids, hesperidin, narirutin, and ferulic acid. On the other hand, the main components of the orange peel are polyphenolic and flavonoid compounds. The main flavonoids found in orange peel are hesperidine, narirutin, naringin and eriocitrin [43].

Recently we succeeded to prepare nanosized α-MnO_2 as cathode material in lithium batteries by a green synthesis method using extracts of lemon juice and peel [44] extracts of green and black tea as biological reducing agents [44,45]. These methods are cost effective, eco-friendly and scalable methods which reduce the cost and hazardous impact of traditional chemical methods.

In this study we use also green synthesis route to prepare MnO_2 and test it as an electrode material for supercapacitors. We use low cost extracts of juice and peel of oranges as reducing agents to prepare nanosized MnO_2. The as-prepared samples were characterized by X-ray powder diffraction, thermal analysis (TG), surface area measurements, High resolution transmission electron microscope (HRTEM) and electrochemical testing as electrodes for supercapacitors.

2. Experimental

Extracts of orange's juice and peel were used as reducing agents to reduce $KMnO_4$ to prepare two samples of MnO_2. OJ-MnO_2 sample was prepared through redox reaction between $KMnO_4$ and extract of orange's juice. This extract was obtained from the fresh orange, which, washed, peeled and squeezed to obtain filtered clear extract.

Acidified 100 ml solution of 3 g $KMnO_4$ by 2 ml of 2.5 M H_2SO_4 was mixed with the above mentioned extract through drowsily addition of

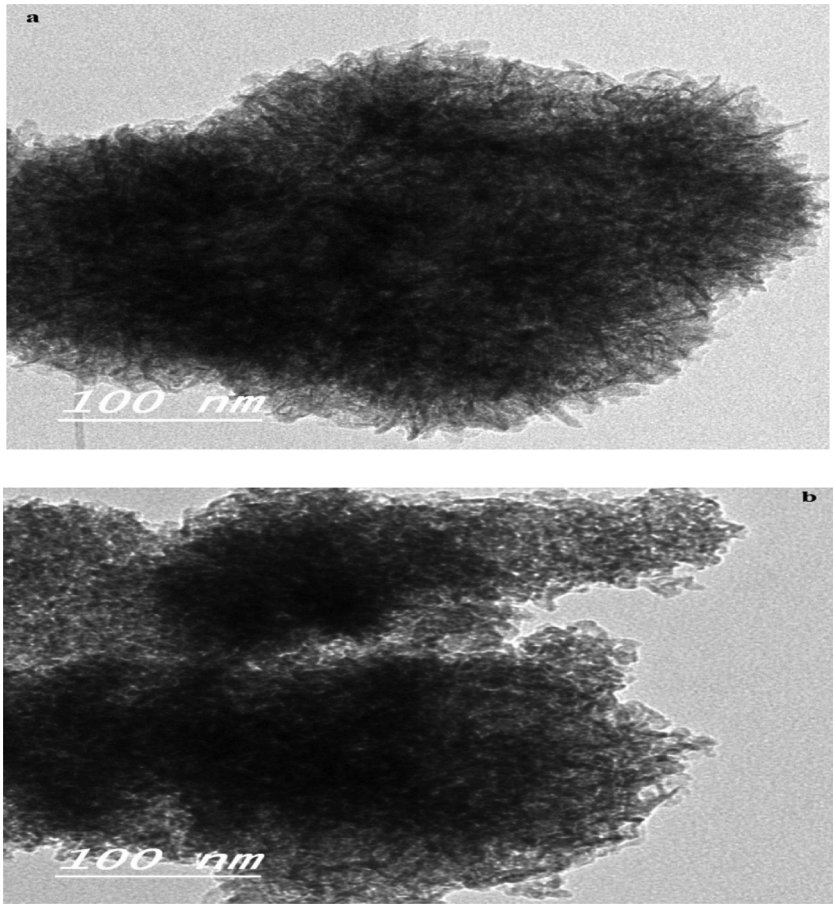

Fig. 3. TEM images of green synthesized a) OJ-MnO_2 and b) OP-MnO_2.

the extract. The color of the stirring mixture changes rapidly from violet to black upon the addition of the juice extract due to the complete reduction of $KMnO_4$ by orange's juice extract. The solution was stirred for 1 h at room temperature. The black precipitate was isolated by filtration with successive washing by distilled water several times to decrease the expected K^+ % in the precipitate. The collected precipitate was dried overnight at 90 °C then calcined at 300 °C for 5 h at an ambient atmosphere.

The same method mentioned above was used to prepare OP-MnO_2 using the extract of orange's peel to reduce acidified solution of 3 g $KMnO_4$. The clear extract was obtained from cleaned, sliced, boiled and filtered orange's peel. Here the change of the color from violet to black is slow.

XRD patterns were recorded using Philips X'Pert apparatus equipped with a CuK_α X-ray source (λ = 1.54056 A°) in the 2θ range 10–80°. TGA measurements were carried out using a thermal gravimetric analyzer (Perkin Elmer, TGA 7 series) in the temperature range of 30–800 °C in air at a heating rate of 10 °C/min. Transmission electron microscope, JEOL (TEM, JEM-1230) Japan was used to investigate the morphology of the samples. The specific surface area was measured by nitrogen adsorption/desorption at 77 K using BET method (Quantachrome NOVA Automated Gas Sorption). Electrochemical properties were measured by Potentiostat Autolab 302 N electrochemical workstation (Metrohm).

The electrochemical measurements cyclic voltammetry (CV), charge and discharge (CD), and cycling stability were carried out in three-electrode cell system with a glassy carbon (GC) electrode as a working electrode. A Pt wire and Ag/AgCl electrode (3 M KCl) were used as a counter electrode and a reference electrode, respectively. Prior to use, the GC electrode was polished with 0.3 μm alumina to create a mirror surface. The catalyst was prepared by dispersing 2.5 mg of the active material in 0.5 ml mixture solution of (Nafion® 117 (5%): Ethanol: H_2O, 10: 20: 70, respectively) by ultrasonication for 30 min A 5 μl suspension of the active material was coated onto the glassy carbon electrode. Finally, the working electrode was dried at 60 °C for 10 min and left to be cooled down.

3. Results and discussion

It is worth noting that during the synthesis of these oxides OJ- MnO_2 formed very rapidly after addition the extract of orange's juice to the solution of $KMnO_4$. Rapid conversion of violet solution of $KMnO_4$ to black precipitate of MnO_2 upon addition of the extract of orange's juice is an indication of rapid reaction and formation of MnO_2. On the contrary upon addition of the extract of orange's peel to the violet solution of $KMnO_4$, slow reaction was noticed from slow conversion of violet solution of $KMnO_4$ to black precipitate of MnO_2. This difference in the reaction rate is attributed to the difference in strength in reducing characters in the two extracts. Due to various constituents in the extract of orange juice it has stronger reducing ability than that of orange peel [43]. It seems that the difference in the speed of formation of each oxide affected the % of K^+ ions trapped in the MnO_2 tunnel. The higher amount of potassium located in case of OJ-MnO_2 came from rapid redox reaction between the juice of orange and $KMnO_4$. This fast formation of MnO_2 did not give chance for K ions to release from trapping inside the tunnel. On the contrary OP- MnO_2 took time to be formed through the redox reaction between the extract of peel of orange and $KMnO_4$. This slow reaction rate gave potassium ions the opportunity to liberate from trapping inside the tunnel of MnO_2.

OP-MnO_2 showed little % of K^+ ions as estimated from chemical

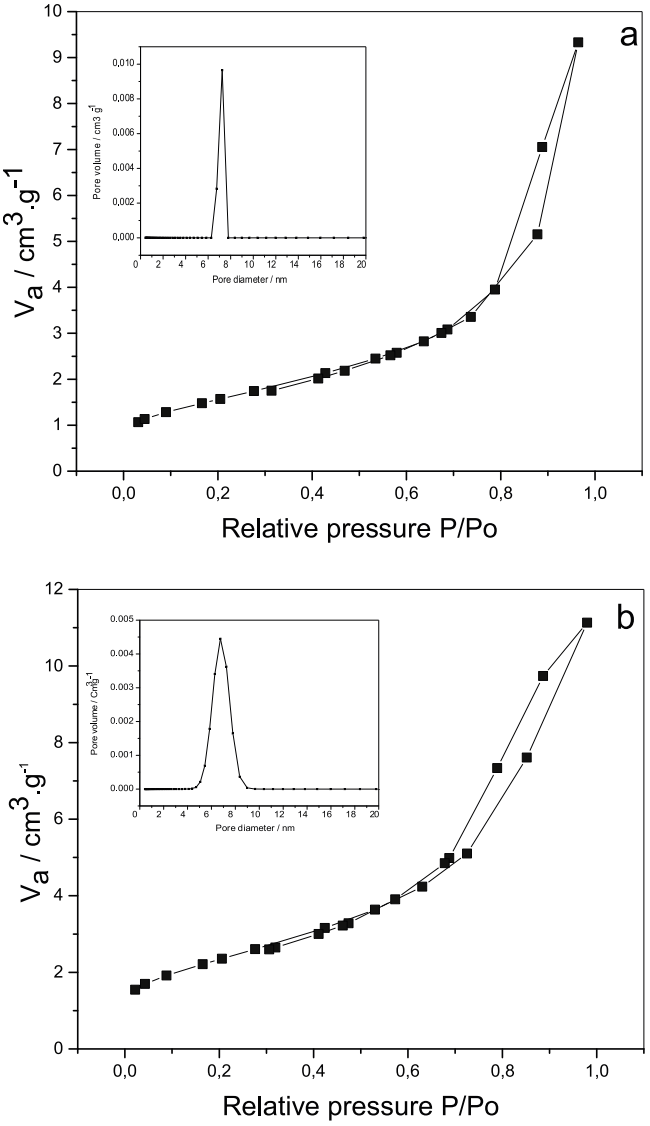

Fig. 4. N_2 adsorption-desorption isotherms and the pore size distribution (PSD) curves (insets) of a) OJ-MnO_2 and b) OP-MnO_2.

Table 1
The porous structural data of the prepared samples.

Sample	BET surface Area ($m^2. g^{-1}$)	Average pore size (nm)
OJ-MnO_2	5.63	7.25
OP-MnO_2	8.40	6.75

analysis by inductively coupled plasma (ICP) to form $K_{0.06}MnO_2$. ICP analysis showed higher % of K^+ ions in case of OJ-MnO_2 which formed rapidly so more amount of potassium ions was trapped inside 2*2 tunnel of MnO_2 to form $K_{0.15}MnO_2$.

The crystal structures of the green synthesized oxides using extract of orange peel OP-MnO_2 and extract of orange juice OJ-MnO_2 were detected by X-ray powder diffraction (XRD). XRD of the as prepared samples shown in Fig. 1(a and b) have the main characteristic peaks of α-MnO_2 according to (JCPDS no.44-0141). One of the main characteristic peaks located at 2θ = 37° is pronounced in both samples and assigned to (211) reflection of α-MnO_2 as reported also in our previous work [44–46]. The other broad peaks are well observed and attributed also to the structure of α-MnO_2. These broad peaks reflect the nanosized structure of the as prepared samples as will mention in TEM section.

We reported in our previous studies [44–46] that the strength of the reducing agent can control K^+ content inserted in the 2 × 2 cavities of α-MnO_2. This potassium content plays significant role in the stabilization of α-MnO_2 lattice. The higher disordered material resulting from less active reducing agent has less K^+ content in the tunnel of α-MnO_2 structure.

Fig. 2 shows thermogravimetric analyses (TGA) of the as-prepared samples OJ-MnO_2 and OP-MnO_2 respectively. Three remarkable weight losses can be detected clearly entire the range 30–1000 °C. The first weight loss recognized in both samples OJ-MnO_2 and OP-MnO_2 was observed up to 200 °C is attributed to the removal of physically adsorbed water on surface of MnO_2. Removal of structural water and hence reduction of MnO_2 to Mn_2O_3 through loss of oxygen can be observed from the second weight loss between 400–500 °C [45].The third weight loss for OP-MnO_2 started at about 650 °C and went gradually is attributed to further oxygen loss and the formation of the Mn_3O_4 spinel structure [46]. In case of OJ-MnO_2 sample this further conversion from Mn_2O_3 to Mn_3O_4 observed at higher temperature above 850 °C, this may attribute to high percent of potassium ions in this sample.

According to the TEM images shown in Fig. 3 we can notice very fine interconnected nanowires. As we can see clearly the lengths and diameters of these nanwires are in nanometer scale. These nano materials are expected to have high surface area which will affect positively on the electrochemical performance.

Fig. 4, displays N_2- adsorption–desorption isotherms and pore-size distributions of OJ-MnO_2 and OP-MnO_2 prepared by green synthesis method. Both isotherms of these two samples are matched well with type IV with hysteresis loop H3 [47]. This type according to IUPAC-classification is characteristic to adsorption on mesopores solids [48]. The mesopores nature of the prepared oxides can be confirmed from the inset in Fig. 4. The pore size distributions of both samples show that the peaks centered at 7.25 and 6.75 nm for OJ-MnO_2 and OP-MnO_2, respectively confirm the presence of mesoporous particles as they centered in the range from 2 to 50 nm. Calculated surface area for both samples according to Barrett_Joyner_Halenda method are 5.63 and 8.40 $m^2. g^{-1}$ for OJ-MnO_2 and OP-MnO_2, respectively as shown in Table 1.

Cyclic voltammetry (CV) was performed to determine the specific capacitance (SC) of MnO_2 in the potential range of −0.2 V to 1.2 V vs. Ag/AgCl in 0.5 M Na_2SO_4 electrolyte at a scan rate of 100 mV/s, as shown in Fig. 5**(C)**. The CV profiles of the prepared samples maintained a non-rectangular shape with some peaks, indicating the pseudocapacitive behavior of all samples [49]. The observed peaks in the potential range from 0 V to 1 V were ascribed to redox reactions [50]. The anodic peak which appear in the potential range 0.8–1 V might be attributed to the oxidation mechanism that is described in Eqs. (1)–(3) [51].

$$Mn^{2+} \rightarrow Mn^{3+} + e^- \quad (1)$$

$$Mn^{3+} + 2H_2O \rightarrow MnOOH + 3H^+ \quad (2)$$

$$MnOOH \rightarrow MnO_2 + H^+ + e^- \quad (3)$$

While the peak in the region 0.2–0.4 V indicates the oxidation reaction of Mn(III) to Mn(IV) species or Mn(II) to Mn(III) species. The broad cathodic peak in the potential range 0.3-0.8 V may be related to the reduction of MnO_2 to MnOOH, which is subsequently reduced to Mn (II) [52].

The specific capacitance (C_{sp}) of the active materials was calculated from charging and discharging measurements (CD) (Fig. 6(a), (b)) through the following equation.

$$C_{sp} = \frac{I\Delta t}{m\,\Delta V}$$

where I is the discharged current (A), Δt is the discharged time (s), m is the total weight of samples coated on glassy carbon electrode, and ΔV is the potential range (V). The specific capacitance values of the OJ-MnO_2 sample is 18.5, 25, 33, and 50 F/g at current densities 15, 5, 2, 0.5 A/g

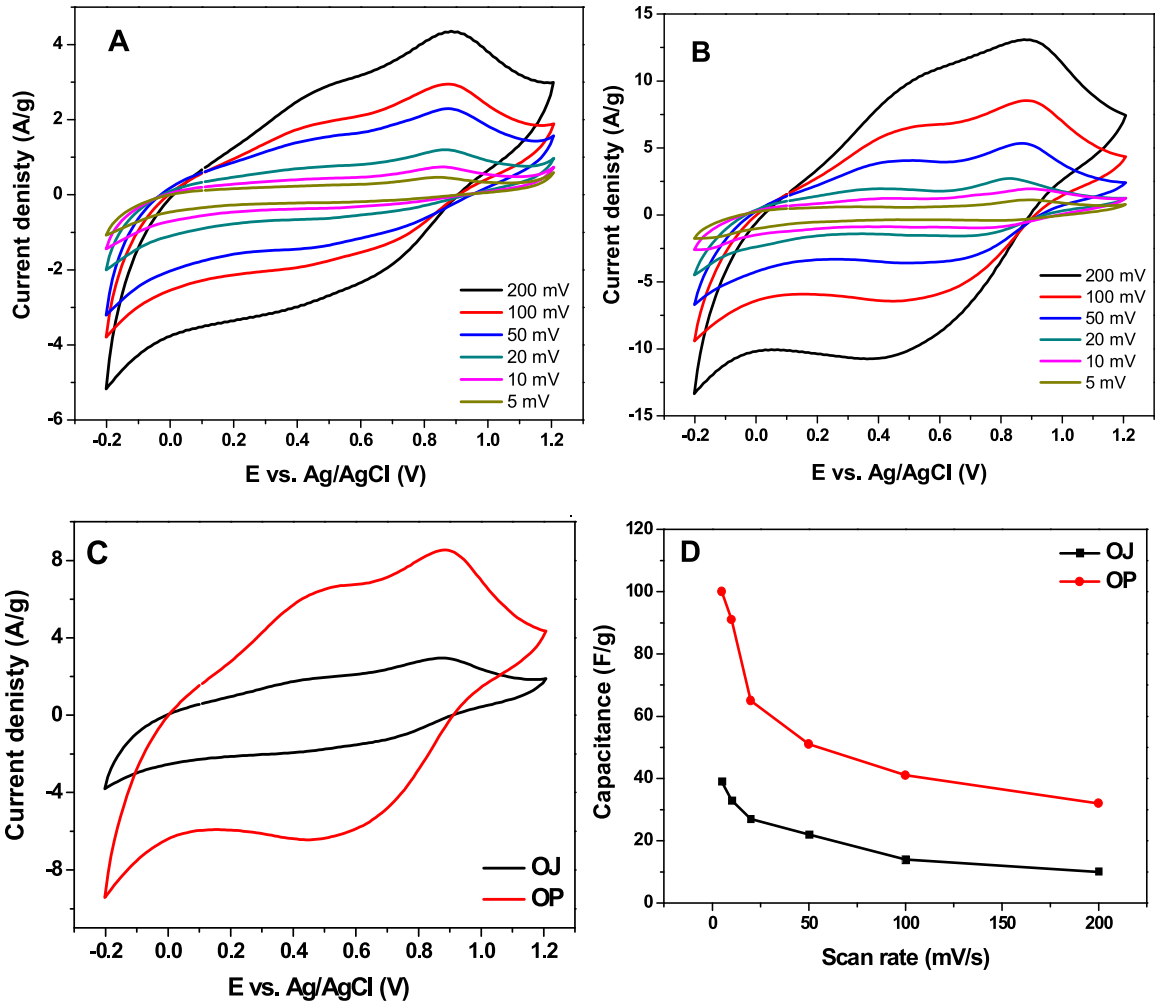

Fig. 5. CV curves of samples **(A)** OJ-MnO_2 and **(B)** OP-MnO_2 at different scan rates from 5 to 200 mV/s **(C)** CV at 80 mV/s, in 0.5 M Na_2SO_4**(D)** C_{sp} versus scan rates.

respectively. While the capacitance of OP-MnO_2 sample is 61, 85, 107, and 139 F/g at the same current densities. The capacitances of OP-MnO_2 are more than two times and half that obtained for OJ-MnO_2 at the same current densities.

The cycling stability is an important requirement for electrochemical supercapacitors [53,54]. The stability tests of OP-MnO_2 electrodes was performed at current density of 3 A/g for 500 cycles using charge/discharge technique in the potential windows ranging from -0.2 to 1.2 V. Fig. 7 shows that the capacitance retention slightly increases during the first 450 cycles compared to the first cycle. Then, the electrode retrieved its capacitance at cycle 500 (1st cycle was 119 F/g, while it becomes 137 F/g with 115% capacitance retention at 350th cycle, and at 500th cycle was 119 F/g with 100% capacitance retention).

The capacitances of OP-MnO_2 are almost between two to three times higher than those observed for OJ-MnO_2 at different current densities. This remarkable higher capacitance for OP-MnO_2 sample in comparison with that of OJ-MnO_2 sample may attribute to two postulations. The first one is the higher surface area and small particle size of OP-MnO_2 sample as noticed from BET surface area data (shown in Table 1). The second postulation is the amount of K trapped inside the 2*2 tunnel of alpha MnO_2. The inductively coupled plasma analysis (ICP) used to detect potassium showed that it is higher in case of OJ-MnO_2 as stated previously. This higher inactive potassium content in case of OJ-MnO_2 decrease the entire capacitance of this sample in comparison with OP-MnO_2 which has lower K^+ % and shows higher capacitance. This electrochemical behavior in supercapacitor is in a good agreement with the electrochemical behavior in lithium batteries for MnO_2 prepared from extracts of green and black tea, respectively [45]. In this previous work [45] extract of green tea as reducing agent is stronger than that of black tea. So it reduced $KMnO_4$ faster than the extract of black tea. This very fast preparation MnO_2 using extract of green tea did not allow a complete removal of K ions, despite several washings with distilled water. This means that the synthesis process is affected by the strength of the reducing agent, which governs the ionic extraction from the 2*2 cavities and controls the diffusion of K ions. As an experimental result, the redox reaction assisted by black tea is not as fast as with green tea, because of the difference in the flavonoid structure and the strength of the antioxidant species. The sample synthesized using black tea showed better initial capacity (~230 mA h /g) than the sample synthesized using green tea GT-MnO_2 (~160 mA h / g) [45]. Here in this study the OJ-MnO_2 which formed very fast has higher % of K ions inside 2*2 tunnel and hence affected the initial capacitance value. On the contrary OP-MnO_2 yielded higher capacitances as mentioned above at the same current densities. Higher % of K ions inside 2*2 impede the easy insertion and extraction of H^+ in and out of this tunnel. Also these K ions are inactive constituents which reduce the entire capacitance value as in case of OJ-MnO_2. To the best of our knowledge this is the first trial to use MnO_2 prepared by green synthesis method as storage material in supercapacitors. Further modifications for these prepared oxides are required e.g. loading in some polymers for further improvement in the electrochemical properties.

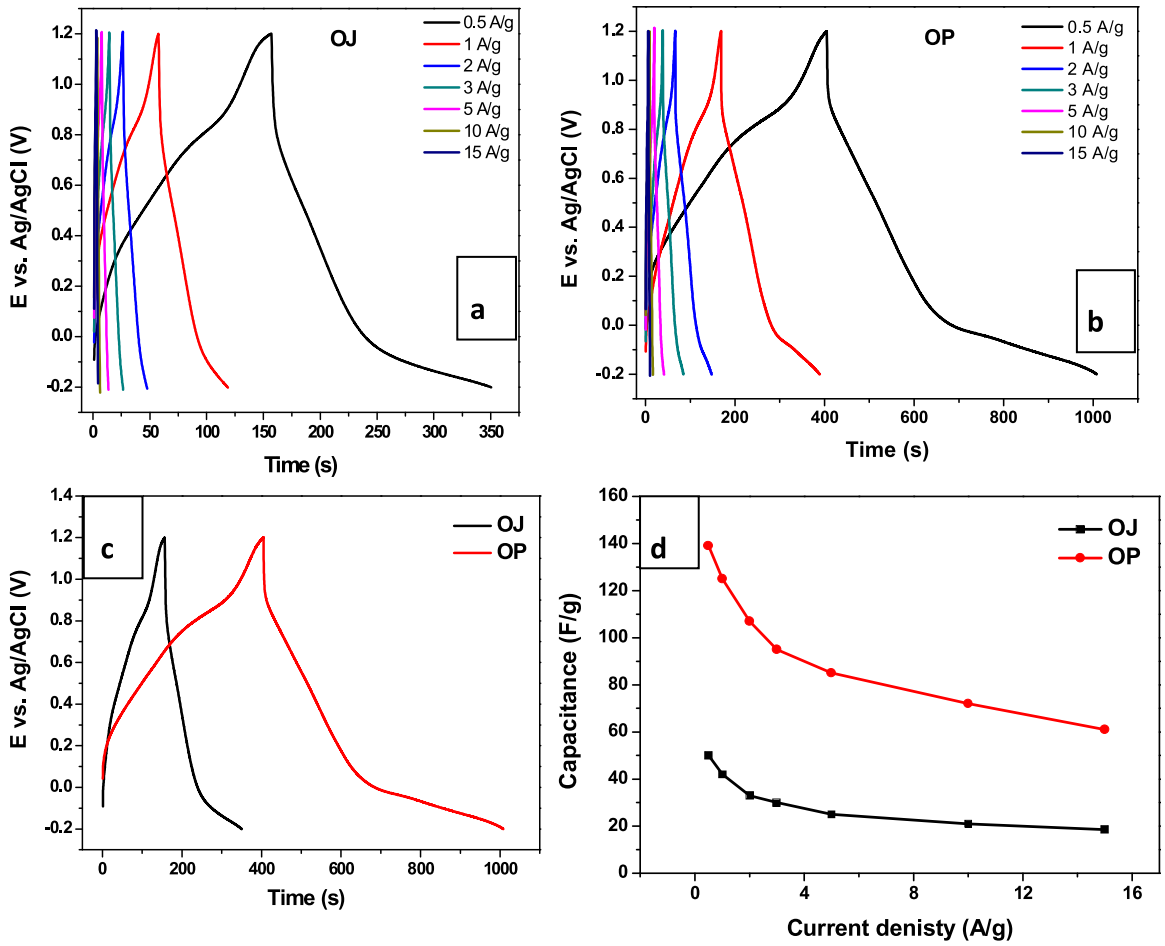

Fig. 6. (a) and (b) Galvanostatic charge/discharge characteristics of the MnO_2 in 0.5 M Na_2SO_4 at different current densities (c) charge/discharge curves at 0.5 A/g, and (d) C_{sp} versus current densities.

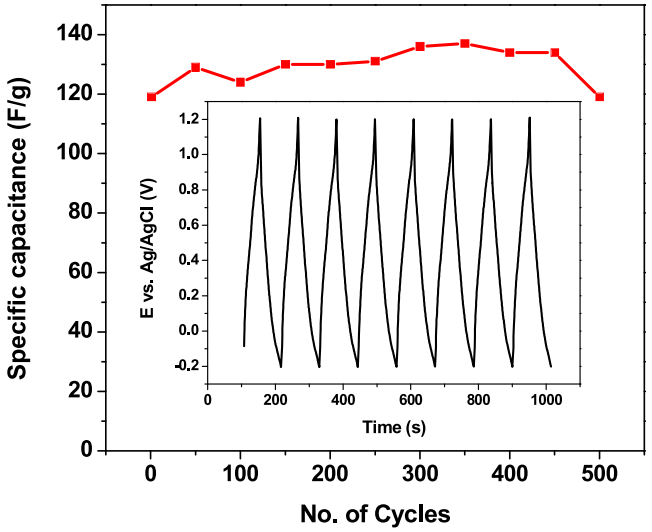

Fig. 7. Cycling stability of OP-MnO_2 at 3 A/g for 500 cycles.

4. Conclusion

Two nanosized α-MnO_2 oxides were successfully prepared by an economical and eco-friendly green synthesis method using extracts of orange juice and peel as biological antioxidants reagents. Both oxides have very fine interconnected nanowires as revealed from TEM investigation. Sample prepared by using the extract of orange peel (OP-MnO_2) has higher surface area and lower K content than that prepared using extract of orange juice (OJ-MnO_2). Higher surface area and lower K content in OP-MnO_2 is positively reflected on its electrochemical properties. OP-MnO_2 shows higher capacitance (two times and half at current density 0.5 A/g) than OJ-MnO_2. This was a preliminary trial to test synthesized MnO_2 using waste of orange (orange peel) in capacitor and forthcoming work will concentrate on modification of such prepared oxide as potential electrode material for capacitor.

Acknowledgment

The authors are grateful for financial support from National Research center.

References

[1] D. Hou, H. Tao, X. Zhu, M. Li, Polydopamine and MnO_2 core-shell composites for high-performance supercapacitors, Appl. Surf. Sci. 419 (2017) 580–585.
[2] F. Zhu, Yu Liu, M. Yan, W. Shi, Construction of hierarchical $FeCo_2O_4$@MnO_2 core-shell nanostructures on carbon fibers for high-performance asymmetric supercapacitor, J. Colloid Interface Sci. 512 (2018) 419–427.
[3] S.S. Xu, D.M. Yang, F. Zhang, J.C. Liu, A.R. Guo, F. Hou, Fabrication of $NiCo_2O_4$ and carbon nanotube nanocomposite films as a high-performance flexible electrode of supercapacitors, RSC Adv. 5 (2015) 74032–74039.
[4] K. Wang, H.P. Wu, Y.N. Meng, Z.X. Wei, Conducting polymer nanowire arrays for high performance supercapacitors, Small 10 (2014) 14–31.
[5] J. Xu, J. Li1, Q. Yang, X. Yan, Ch. Chen, In-situ synthesis of MnO_2@Graphdiyne oxides nanocomposite with enhanced performance of supercapacitors, Electrochim. Acta 251 (2017) 672–680.
[6] N. Li, X.H. Zhu, C.Y. Zhang, L.Q. Lai, R. Jiang, J.L. Zhu, Controllable synthesis of different microstructured MnO_2 by a facile hydrothermal method for supercapacitors, J. Alloys. Compd. 692 (2017) 26–33.

[7] N. Goubard-Bretesche, O. Crosnier, G. Buvat, F. Favier, T. Brousse, Electrochemical study of aqueous asymmetric $FeWO_4/MnO_2$ supercapacitor, J. Power Sources 326 (2016) 695–701.

[8] Y.C. Xiong, M. Zhou, H. Chen, L. Feng, Z. Wang, X.Z. Yan, S.Y. Guan, Synthesis of honeycomb MnO_2nanospheres/carbon nanoparticles/graphene composites as electrode materials for supercapacitors, Appl. Surf. Sci. 357 (2015) 1024–1030.

[9] K.O. Oyedotun, M.J. Madito, D.Y. Momodu, A.A. Mirghni, T.M. Masikhwa, N. Manyala, Synthesis of ternary NiCo-MnO_2 nanocomposite and its application as a novel high energy supercapattery device, Chem. Eng. J. 335 (2018) 416–433.

[10] F. Zhang, T. Zhang, X. Yang, L. Zhang, K. Leng, Y. Huang, Y. Chen, A high-performance supercapacitor-battery hybrid energy storage device based on graphene enhanced electrode materials with ultrahigh energy density, Energy Environ. Sci. 6 (2013) 1623.

[11] J. Xu, S. Dou, H. Liu, L. Dai, Cathode materials for next generation lithium ion batteries, Nano Energy 2 (4) (2013) 439–442.

[12] P.E. Lokhande, Synthesis and characterization of Ni.Co(OH)2 material for supercapacitor application, Int. Adv. Res. J. Sci Eng. Technol. 2 (9) (2015) 10–13.

[13] X. Wang, X. Fan, G. Li, M. Li, X. Xiao, A. Yu, Z. Chen, Composites of MnO_2 nanocrystals and partially graphitized hierarchically porous carbon spheres with improved rate capability for high-performance supercapacitors, Carbon N. Y. 93 (2015) 258–265.

[14] S. Trana, K. Malika Tripathia, K. Bit Na, Y. In-Kyu, B. Jun Parkc, Y. Hee Hanc, T. Kim, Three-dimensionally assembled Graphene/α-MnO_2 nanowire hybrid hydrogels for high performance supercapacitors, Mater. Res. Bull. 96 (2017) 395–404.

[15] Z. Hu, L. Zu, Y. Jiang, H. Lian, Y. Liu, Z. Li, F. Chen, X. Wang, X. Cui, High specific capacitance of Polyaniline/Mesoporous manganese dioxide composite using KI-H_2SO_4 electrolyte, Polymers 7 (2015) 1939–1953.

[16] M. Huang, Y.X. Zhang, F. Li, L.L. Zhang, Z.Y. Wen, Q. Liu, Facile synthesis of hierarchical $Co_3O4@MnO_2$ core shell arrays on Ni foam for asymmetric supercapacitors, J. Power Sources 252 (2014) 98–106.

[17] Q.H. Wang, L.F. Jiao, H.M. Du, Y.J. Wang, H.T. Yuan, Fe_3O_4nanoparticles grown on graphene as advanced electrode materials for supercapacitors, J. Power Sources 245 (2014) 101–106.

[18] M.X. Liu, J.S. Qian, Y.H. Zhao, D.Z. Zhu, L.H. Gan, L.W. Chen, Core–shell ultra microporous@microporous carbon nanospheres as advanced supercapacitor Electrodes, J. Mater. Chem. A 3 (2015) 11517–11526.

[19] L. Lu, Sh. Xu, J. An, Sh. Yan, Electrochemical performance of CNTs/RGO/MnO_2 composite material for supercapacitor, Nanomater. Nanotechnol. 6 (2016) 1–7.

[20] Q. Li, J.J. He, D.Q. Liu, H.W. Yue, S. Bai, B.L. Liu, L.L. Gu, D.Y. He, Facile preparation of hovenia-acerba-like hierarchical MnO_2/C composites and their excellent energy storage performance for supercapacitors, J. Alloys. Compd. 693 (2017) 970–978.

[21] R. Samal, B. Dash, C.K. Sarangi, K. Sanjay, D.T. Subbaiah, G. Senanayak, M. Minakshi, Influence of synthesis temperature on the growth and surface morphology of Co_3O_4 nano cubes for supercapacitor applications, Nanomaterials 7 (356) (2017) 1–13.

[22] R. Thangappan, M. Arivanandhan, R. Dhinesh Kumar, R. Jayavel, Facile synthesis of RuO_2 nanoparticles anchored on graphene nanosheets for high performance composite electrode for supercapacitor applications, J. Phys. Chem. Solids 121 (2018) 339–349.

[23] N.M. Ndiaye, B.D. Ngom, N.F. Sylla, T.M. Masikhwa, M.J. Madito, D. Momodu, T. Ntsoane, N. Manyala, Three dimensional vanadium pentoxide/graphene foam composite as positive electrode for high performance asymmetric electrochemical supercapacitor, J. Colloid Interface Sci. 532 (2018) 395–406.

[24] D.J. Ahirrao, K. Mohanapriya, N. Jha, V_2O_5 nanowires - graphene composite as an outstanding electrode material for high electrochemical performance and long-cycle- life supercapacitor, Mater. Res. Bull. 108 (2018) 73–82.

[25] M. Huang, Y.X. Zhang, F. Li, L.L. Zhang, R.S. Ruoff, Z.Y. Wen, Q. Liu, Self-assembly of mesoporous nanotubes assembled from inter wove nultrathin birnessite-type MnO_2 nanosheets for asymmetric supercapacitors, Sci. Rep. 4 (2014) 3878–3886.

[26] T. Brousse, D. Belanger, J.W. Long, To be or not to be pseudo capacitive? J. Electrochem. Soc. 162 (2015) A5185–A5189.

[27] L. Pan, K.X. Wang, X.D. Zhu, X.M. Xie, Y.T. Liu, Hierarchical assembly of SnO_2 nanowires on MnO_2 nanosheets: a novel 1/2D hybrid architecture for high capacity, reversible lithium storage, J. Mater. Chem. A 3 (2015) 6477–6483.

[28] S.X. Deng, D. Sun, C.H. Wu, H. Wang, J.B. Liu, Y.X. Sun, H. Yan, Synthesis and electrochemical properties of MnO_2 nanorods/graphene composites for supercapacitor applications, Electrochim. Acta 111 (2013) 707–712.

[29] A.J. Paleoa, P. Staiti, A. Brigandì, F.N. Ferreira, A.M. Rocha, F. Lufrano, Supercapacitors based on AC/MnO_2 deposited onto dip-coated carbon nanofiber cotton fabric electrodes, Energy Storage Mater. 12 (2018) 204–215.

[30] T.H. Wu, D. Hesp, V. Dhanak, C. Collins, F. Braga, L.J. Hardwick, C.C. Hu, Charge storage mechanism of activated manganese oxide composites for pseudocapacitors, J. Mater. Chem. A 3 (2015) 12786–12795.

[31] P. Staiti, F. Lufrano, Investigation of polymer electrolyte hybrid supercapacitor based on manganese oxide-carbon electrodes, Electrochim. Acta 55 (2010) 7436–7442.

[32] Yu Li, Z. Xu, D. Wang, J. Zhao, H. Zhang, Snowflake-like core-shell α-MnO_2@ δ-MnO_2 for high performance asymmetric supercapacitor, Electrochim. Acta 251 (2017) 344–354.

[33] J. Zhang, Y.D. Cao, C.A. Wang, R. Ran, Design and preparation of MnO_2/CeO_2-MnO_2 double-shelled binary oxide hollow spheres and their application in CO Oxidation, ACS Appl. Mater. Inter. 8 (2016) 8670–8677.

[34] S.W. Bian, Y.P. Zhao, C.Y. Xian, Porous MnO_2 hollow spheres constructed by nanosheets and their application in electrochemical capacitors, Mater. Lett. 111 (2013) 75–77.

[35] S.F. Chin, S.C. Pang, M.A. Anderson, Self-assembled manganese dioxide nanowires as electrode materials for electrochemical capacitors, Mater. Lett. 64 (2010) 2670–2672.

[36] H.T. Guan, Y.D. Wang, G. Chen, J. Zhu, frequency and temperature effects on dielectric and electrical characteristics of α-MnO_2nanorods, Powder Technol. 224 (2012) 356–359.

[37] D. Yan, S. Cheng, R.F. Zhuo, J.T. Chen, J.J. Feng, H.T. Feng, H.J. Li, Z.G. Wu, J. Wang, P.X. Yan, Synthesis, characterization, and microwave absorption property of the SnO_2 nanowire/paraffin composites, Nanoscale Res. Lett. 4 (2009) 1452–1457.

[38] Y.S. Ding, X.F. Shen, S. Sithambaram, S. Gomez, R. Kumar, V.M.B. Crisostomo, S.L. Suib, M. Aindow, Synthesis and catalytic activity of cryptomelane-type manganese dioxide nanomaterials produced by a novel solvent-free method, Chem. Mater. 17 (2005) 5382–5389.

[39] H. Guan, J. Xie, G. Chen, Y. Wang, Facile synthesis of α-MnO_2nanorods at low temperature and their microwave absorption properties, Mater. Chem. Phys. 143 (2014) 1061–1068.

[40] J.A. Linthorst, An overview: origins and development of green chemistry, Theor. Found. Chem. Eng. 12 (2010) 55–68.

[41] A.E. Hegazy, M.I. Ibrahium, Antioxidant activities of orange peel extracts, World Appl. Sci. J. 18 (5) (2012) 684–688.

[42] G. Mandalari, R.N. Bennett, G. Bisignano, A. Saija, G. Dugo, C.B. Faulds, K.W. Waldron, Characterization of flavonoids and pectin from bergamot (Citrus bergamia Risso) peel, a major byproduct of essential oil extraction, J. Agric. Food Chem. 54 (2006) 197–203.

[43] V.A. Bampidis, P.H. Robinson, Citrus byproducts as ruminant feeds: a review, Anim. Feed Sci. Technol. 128 (3/4) (2006) 175–217.

[44] A.M. Hashem, H. Abuzeid, M. Kaus, S. Indris, H. Ehrenberg, A. Mauger, C.M. Julien, Green synthesis of nanosized manganese dioxide as positive electrode for lithium-ion batteries using lemon juice and citrus peel, Electrochim. Acta 262 (2018) 74–81.

[45] H.M. Abuzeid, A.M. Hashem, M. Kaus, M. Knapp, S. Indris, H. Ehrenberg, A. Mauger, C.M. Julien, Electrochemical performance of nanosized MnO_2 synthesized by redox route using biological reducing agents, J. Alloys. Compd. 746 (2018) 227–237.

[46] A.M. Hashem, H.M. Abuzeid, A.E. Abdel-Ghany, A. Mauger, K. Zaghib, C.M. Julien, SnO_2–MnO_2 composite powders and their electrochemical properties, J. Power Sources 202 (2012) 291–298.

[47] S.J. Gregg, K.S.W. Sing, Adsorption, Surface Area and Porosity, 2nd ed., Academic Press, London, 1982.

[48] P. Yuan, D. Liu, M.D. Fan, D. Yang, R.L. Zhu, Removal of hexavalent chromium [Cr (VI)] from aqueous solutions by the diatomite-supported/unsupported magnetite nanoparticles, J. Hazard. Mater. 173 (2010) 614–621.

[49] L. Wen-Zhi, L. You-Qin, H. Guang-Qi, Preparation of manganese dioxide modified glassy carbon electrode by a novel film plating/cyclic voltammetry method for H_2O_2 detection, J. Chil. Chem. Soc. 54 (4) (2009) 366–371.

[50] O. Bricker, Some stability relations in the system Mn-O_2-H_2O at 25° and one atmosphere total pressure, Am. Mineral. 50 (9) (1965) 1296–1354.

[51] S.D. Kim, D. Lim, D. Nam, D. Seo, S.E. Shim, S.H. Baeck, Synthesis of Manganese Oxide for Supercapacitors: Effect of Precursor on Electrocatalytic Performance, J. Nanosci. Nanotechnol. 1;17 (11) (2017) 7947–7951.

[52] Y. Shen, R. Zerger, R. DeGuzman, S. Suib, L. McCurdy, D. Potter, C. O'Young, Manganese oxide octahedral molecular sieves: preparation, characterization, and applications, Science 260 (5107) (1993) 511–515.

[53] W. Wei, X. Cui, W. Chen, D.G. Ivey, Manganese oxide-based materials as electrochemical supercapacitor electrodes, Chem. Soc. Rev. 40 (3) (2011) 1697–1721.

[54] D.M. El-Gendy, N.A. Ghany, E.F. El Sherbini, N.K. Allam, Adenine-functionalized spongy graphene for green and high-performance supercapacitors, Sci. Rep. 20 (7) (2017) 43104.